Natural Hazards (2025) 121:12169–12193
https://doi.org/10.1007/s11069-025-07276-2

ORIGINAL PAPER

Modelling emplacement of the world's largest tsunami boulder

Koki Nakata[1] · **Masashi Watanabe**[2] · **Kazuhisa Goto**[1]

Received: 13 October 2024 / Accepted: 7 April 2025 / Published online: 9 May 2025

Abstract

Large tsunami waves have struck the Sakishima Islands of Japan repeatedly. The latest was the 1771 Meiwa tsunami (> 25 m run-up height), which was generated by an earthquake along the Ryukyu Trench. Numerous tsunami boulders lie along the coastlines of these islands. The largest tsunami boulder of the Sakishima Islands, called "*Obi-iwa*", is located on the west coast of Shimoji Island on a ca. 12 m high cliff. Historical documents imply that it was transported by the Meiwa tsunami. Nevertheless, whether this boulder could have been transported by the Meiwa tsunami has not been evaluated definitively. Furthermore, the possibility exists that it was transported by a larger and older tsunami generated along the Ryukyu Trench or by an unknown large tsunami originating from the Okinawa Trough. For this study, we conducted 3D measuring of this boulder using LiDAR equipment and used boulder transport models to evaluate whether the Meiwa tsunami could have transported it. From 3D measurements, the weight of this boulder was estimated as approximately 3400 tons: the world's heaviest tsunami boulder reported to date. The boulder transport calculations suggest that the Meiwa tsunami could have transported this boulder, which implies that the assumption of some unknown large tsunami event is unnecessary to explain this boulder's deposition.

Keywords 1771 Meiwa tsunami · Boulder transport model · Cliff-top boulder · LiDAR · Ryukyu Trench · Tsunami boulder

✉ Koki Nakata
nakata-koki864@g.ecc.u-tokyo.ac.jp

Masashi Watanabe
masashi.watanabe@soton.ac.uk

Kazuhisa Goto
goto50@eps.s.u-tokyo.ac.jp

[1] Department of Earth and Planetary Science, The University of Tokyo, 7-3-1 Hongo, Bunkyo-ku, Tokyo 113-0033, Japan

[2] School of Ocean and Earth Science, National Oceanography Centre, University of Southampton, European Way, Southampton SO14 3ZH, UK

1 Introduction

For future tsunami risk assessment, knowing the histories of past tsunami waves, their sizes, and sources are important (e.g., Sugawara 2021). The past tsunami sizes and wave sources can be estimated using tsunami numerical calculations with historical or geological records as constraints. All over the world, many studies have been carried out to elucidate past tsunami sizes and wave sources using this strategy (e.g., Baptista et al. 1998; Satake et al. 2008; Namegaya and Satake 2014; Abad et al. 2020; Lavigne et al. 2021; Nakata et al. 2024).

Especially in the Sakishima Islands, Japan (Fig. 1), plenty of both historical and geological records of past tsunamis are well preserved (Goto et al. 2010). Such records are extremely rare throughout the world. Therefore, the Sakishima Islands are suitable locations to test the degree to which past tsunamis can be identified and characterized (Goto and Shimabukuro 2012).

The Meiwa tsunami (Yaeyama tsunami) struck the Sakishima Islands in 1771, causing tremendous damage and leaving 12,000 victims in its wake (Goto et al. 2010). Damage caused by this tsunami was well recorded in historical documents. For example, historical documents described inundation or a lack of inundation at many locations throughout the Sakishima Islands (Goto et al. 2012). Based on these historical records, the maximum run-up height has been estimated as more than 25 m (Goto et al. 2012). The tsunami wave source has also been estimated using tsunami calculations with the historical records as constraint conditions (Imamura et al. 2001; Nakamura 2009; Miyazawa et al. 2012; Okamura et al. 2018; Nakata et al. 2024). Recently, Nakata et al. (2024) used the latest historical dataset (Goto et al. 2012) as a constraint and re-estimated the wave source model using high-resolution tsunami calculations. They estimated that a large slip (30 m) must occur in a shallow and narrow region of the Ryukyu Trench (30 km fault width, 5 km depth at the fault top) to reproduce the Meiwa tsunami runup distribution estimated from historical records (Fig. 1).

Sandy tsunami deposits have been reported for the Sakishima Islands in geological records (Kawana and Nakata 1994; Nakaza et al. 2013; Okinawa Prefectural Archeological Center

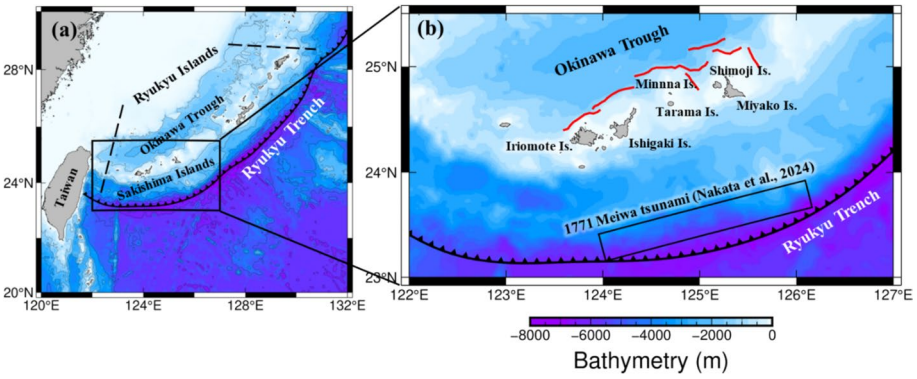

Fig. 1 **a** Map showing the Sakishima Islands, the Ryukyu Islands, the Ryukyu Trench, and the Okinawa Trough locations. **b** Close up map of the Sakishima Islands. The black rectangle shows the location of the Meiwa tsunami fault model by Nakata et al. (2024). The red lines represent the locations of presumed active faults as identified by Izumi et al. (2016). The plate boundary was adapted from Iwasaki et al. (2015)

2017; Ando et al. 2018; Fujita et al. 2020). Especially on Ishigaki and Minna islands (Fig. 1), tsunami deposits predating the Meiwa tsunami have been reported (Okinawa Prefectural Archeological Center 2017; Ando et al. 2018; Fujita et al. 2020). Both islands were struck by large tsunami waves before the 1771 event, about 920–620 years ago. Ando et al. (2018) also found that tsunamis of similar or larger magnitude than the Meiwa tsunami have struck approximately every 600 years during the past 2000 years.

In addition to the sandy tsunami deposits, coral boulders transported by tsunamis, known as tsunami boulders, have also been reported on the Sakishima Islands (e.g., Kawana and Nakata 1994; Goto et al. 2010; Araoka et al. 2013). Araoka et al. (2013) carried out radiocarbon dating of 92 tsunami boulders composed of single massive *Porites* and estimated statistically that the tsunami recurrence interval in the Sakishima Islands is about 150–400 years. Furthermore, these tsunami boulders are useful not only for tsunami age estimation but also for tsunami size and wave source estimation when using boulder transport models (e.g., Hisamatsu et al. 2014; Watanabe et al. 2016). In fact, these tsunami boulders are especially important to estimate the magnitudes and sources of tsunami waves preceding the Meiwa tsunami. For those earlier events, no historical record is available for the Sakishima Islands. For instance, Hisamatsu et al. (2014) applied a boulder transport model (Imamura et al. 2008) for tsunami boulders, called "*Tsunami-ufuishi*" on Ishigaki Island (500 tons; Nakata et al. 2023), and pointed out that at least one tsunami which occurred before the Meiwa tsunami was larger than the Meiwa tsunami.

For this study, we examined only the largest tsunami boulder of the Sakishima Islands, called "*Obi-iwa*" (hereinafter, the OI boulder) (Kato 1989a, b; Goto et al. 2010) among thousands of tsunami boulders of the Sakishima Islands. The OI boulder is located on the west coast of Shimoji Island (Fig. 1) (Kato 1989a, b; Goto et al. 2010). When the boulder was transported to its present location remains unknown, but historical descriptions suggest that it might have been transported by the 1771 Meiwa tsunami (Kato 1989b) because historical records state that a boulder nearly as large as the OI boulder was transported by the Meiwa tsunami to Shimoji Island. Nevertheless, it remains uncertain whether the boulder described in the historical records is indeed the OI boulder, as detailed in Chapter 2 herein. Moreover, the OI boulder is the largest tsunami boulder of the Sakishima Islands. The OI boulder weight is more than ten times that of the known largest tsunami boulder, *Bari-ishi* (216 tons; Watanabe et al. 2016), the transportation of which by the Meiwa tsunami was confirmed using radiocarbon dating and numerical modeling. Therefore, further careful analysis should be carried out to clarify whether the OI boulder was transported by the Meiwa tsunami or by a much larger tsunami. Indeed, Kawana and Nakata (1994) reported that the OI boulder could not have been transported by the Meiwa tsunami but instead by an unknown tsunami originating from the Okinawa Trough (Fig. 1), although they have not evaluated quantitatively whether the OI boulder could not have been transported by the Meiwa tsunami. In this way, the OI boulder might provide very useful information to estimate the size of past large tsunamis striking the Sakishima Islands. Such information is important for future tsunami risk assessment in this area. For this study, we aimed at using numerical calculations to evaluate whether the OI boulder could have been transported by the Meiwa tsunami.

2 *"Obi-iwa"* (The OI boulder)

The OI boulder is located on the west coast of Shimoji Island, at the top of an approximately 12-m-high cliff about 50 m from the shoreline (Fig. 2a–d) (Kato 1989a; Goto et al. 2010). This boulder, which is composed of the Pleistocene Ryukyu limestone, has the same components as those of the cliff. Kato (1989b) estimated its size as 14 × 14 × 9 m, weighing 2500 tons. Kawana and Pirazzoli (1990) estimated it as 16 × 12 × 12 m. Nakaza et al. (2015) estimated its weight as 3700 tons. As the differences between measurement results in each earlier studies suggests, even measurement of the OI boulder is difficult because of its immense size. Its shape and weight are not known precisely. In any case, the OI boulder is at least 20 times heavier than the boulders transported by storm waves in the Ryukyu Islands (Fig. 1) (Goto et al. 2010). In addition, the coast facing the OI boulder has a 200-m-wide coral reef, which can be expected to attenuate any storm wave energy

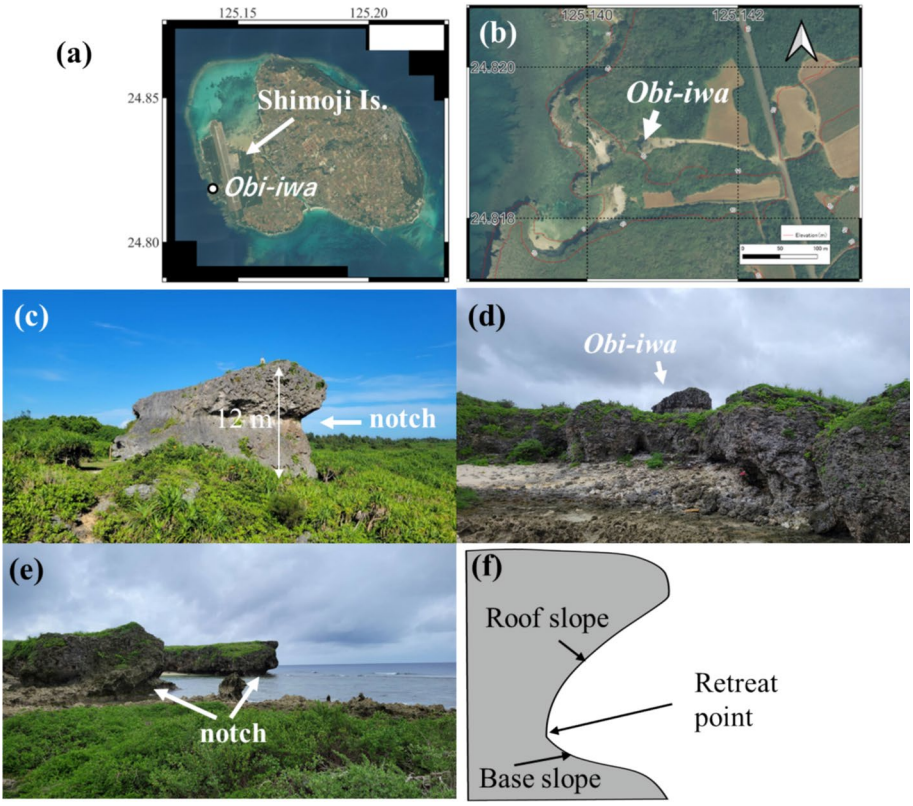

Fig. 2 **a** Satellite photograph of Shimoji Island taken in 2019. This photograph was provided by the Geospatial Information Authority of Japan. **b** Aerial photograph around the OI boulder (white arrow) taken in 2019. This photograph was provided by the Geospatial Information Authority of Japan. **c** File photograph of the OI boulder. The arrow indicates the notch shape. This photograph was taken on June 1, 2022. **d** Field photograph of the OI boulder taken from the bottom of the cliff. This photograph was taken on June 1, 2022. **e** Field photograph of the sea cliff near the OI boulder. The notch was formed on the cliff. This photograph was taken on June 1, 2022. **f** Schematic illustration of the notch. The roof slope is generally longer than the base slope if notches face the open sea. The most caved point is called the "retreat point". This illustration was produced based on information reported by Pirazzoli (1986)

considerably (e.g., Egashira et al. 1985). Therefore, the OI boulder is unlikely to have been transported by storm waves. For the reasons presented above, the OI boulder has been identified as a tsunami boulder (Goto et al. 2010).

Moreover, the OI boulder has a coastal notch shape (Fig. 2c). This notch shape is the origin of the name of the OI boulder. Actually, *Obi* means waist strap in Japanese (Kato 1989a). Coastal notches are indentations cut into the base of coastal cliffs (e.g., Takenaga 1968; Pirazzoli 1986; Trenhaile 2015). Therefore, the OI boulder is expected to have been a part of the coastal cliff originally (Fig. 2e). It has also been pointed out that the OI boulder might have been deposited upside down, as suggested by the notch shape in the OI boulder (Nakaza et al. 2015; Rixhon 2020). Coastal notches formed in moderately exposed sites, such as Shimoji Island (Kawana and Pirazzoli 1990), are particularly prone to being scraped off the top of the notch (roof slope) because of wave splashing; the top of the notch (roof slope) is longer than the bottom of the notch (base slope) (Fig. 2f) (Pirazzoli 1986). However, regarding the notch in the OI boulder, the base slope is longer than the roof slope (Fig. 2c). This feature suggests that the OI boulder was indeed deposited upside down. In addition, karstification is high in the lower part of the notch and low in the upper part (Rixhon 2020). This contrast in karstification is also consistent with overturning of the OI boulder (Rixhon 2020).

Dating of the OI boulder has been conducted by Kato (1989a) and Nakaza et al. (2015). The OI boulder itself is composed of Pleistocene Ryukyu limestone, but its age does not indicate when the tsunami occurred, although dates of attached fresh corals or shells are useful to constrain the tsunami age. Kato (1989a) dated fresh coral fossils attached to the OI boulder surface using radiocarbon dating and reported two ages: 880 ± 70 yr BP and 1280 ± 70 yr BP. Because these age values are not calibrated, we calibrated these ages using Marine20 (Heaton et al. 2020) with the local reservoir effect ($\Delta R = -213 \pm 60$; Hirabayashi et al. 2017). Their calibrated ages are, respectively, 695–315 cal yr BP and 1107–665 cal yr BP. Nakaza et al. (2015) also conducted radiocarbon dating for a *Tridacna* fossil attached to the notch part of the OI boulder and reported AD 1200–1300 for this fossil age. Based on the results presented above, it has been inferred that the OI boulder was located near the shoreline, where shells and corals could attach to the boulder until at least 700 years ago. It was then transported onto the 12 m high cliff top by a tsunami that occurred more recently than 700 years ago. Therefore, the 1771 Meiwa tsunami is one candidate. Also, Ando et al. (2018) and Fujita et al. (2020) reported a tsunami event about 920–620 years ago. Because the tsunami deposits by this event are distributed up to an elevation comparable to that of the Meiwa tsunami deposits, the scale of the tsunami about 920–620 years ago should have been comparable to or greater than that of the Meiwa tsunami (Ando et al. 2018; Fujita et al. 2020). Considering the potential error of age estimation, this event might also be a candidate for transporting the OI boulder.

A legend also suggests that a large tsunami struck Shimoji Island before 1771 (Shimoji 2007; Yamamoto et al. 2014). A historical document called the "*Miyakojima-kiji-shitugi*" introduced this legend. Reportedly, Shimoji Island villages had been destroyed completely by this tsunami. The remains of the villages were still there, but they had not been rebuilt (Shimoji 2007; Yamamoto et al. 2014). The old Japanese map in 1647, called "*Shohokuni-ezu*", described that no one resided on Shimoji Island (Yamamoto et al. 2014). Therefore, this tsunami might have struck before 1647. In addition, another historical document called "*Iyasu-shi-kahu-seitou*" recorded the existence of a chief in villages on Shimoji Island until 1566 (Yamamoto et al. 2014). This document indicates that there were villages and residents until at least 1566. From the records of historical documents described above, this legendary tsunami might have struck in 1566–1647. This age is slightly earlier than the

920–620 years ago event (Ando et al. 2018; Fujita et al. 2020). Therefore, this legendary tsunami might be different from the 920–620 year ago event, although one cannot exclude the possibility that both events are actually the same event.

One historical document, called "*Otoiai-gaki*", indicates that several large boulders equivalent in size to the OI boulder were transported by the 1771 Meiwa tsunami on the coast of Shimoji Island (Kato 1989b). The boulders are described in the document as presented below (Kato 1989b; Sunagawa 1994).

"The big wave transported a boulder with 13.5 m (9 *hiro* in old Japanese unit of length; 1 *hiro* = 1.5 m) height and 60 m (40 *hiro*) perimeter, a boulder with 9.9 m height (6 *hiro* plus 3 *shaku* in old Japanese unit of length; 1 *shaku* = 0.2 *hiro* = 0.3 m), 12 m (8 *hiro*) width, and 18.6 m (12 *hiro* plus 2 *shaku*) length, and a boulder with 6.3 m height (4 *hiro* plus 1 *shaku*), 6.9 m (4 *hiro* plus 3 *shaku*) width, and 12.3 m (8 *hiro* plus 1 *shaku*) length onto the cliff top of 15 m (10 *hiro*) elevation on the south coast of Shimoji Island. In addition, many other boulders with 4.5–6 m (3–4 *hiro*) height and 7.5–9 m (5–6 *hiro*) perimeter were transported onto the cliff top."

The original document described these boulders as located on the south coast of Shimoji Island, but the OI boulder is located on the west coast. However, the height of the cliff on the south coast rises only up to 5 m, whereas > 10 m high cliffs exist only on the west coast (Kato 1989b). In addition, Kawana and Pirazzoli (1990) reported that the relative sea level on Shimoji Island has not changed from 1000 years ago. One can therefore rule out the possibility that the cliffs on the southern coast were the same as those existing (> 10 m high) at the time of the 1771 event. Therefore, Kato (1989b) pointed out that the original document mistakenly referred to the west coast as the south coast. The boulder described first in the document (13.5 m high, 60 m circumference) is of similar size to the OI boulder. For that reason, the possibility exists that the 1771 Meiwa tsunami transported the OI boulder onto the cliff top. Moreover, it is noteworthy that many boulders were deposited near the OI boulder, but these were destroyed during airport construction (Kato 1989b). Therefore, the possibility exists that one of the destroyed boulders was the one described in the historical document.

Kawana and Nakata (1994) speculated that this boulder could not have been transported by the Meiwa tsunami but instead by an unknown tsunami originating from the Okinawa Trough, not the Ryukyu Trench, because this boulder is located on the west coast of Shimoji Island (Fig. 1), which is on the opposite side of the Ryukyu Trench and which faces the Okinawa Trough. Because of such a setting, they suggested that the Okinawa Trough might be the likely tsunami source. Indeed, Izumi et al. (2016) reported the possibility of active faults existing in the Okinawa Trough.

The process of transporting the OI boulder onto the cliff top has not been fully clarified. Two possible processes are that a part of the cliff was transported onto the cliff top directly by the tsunami (Fig. 3a), or that a part of the cliff had already been detached from the cliff and had dropped onto the shallow sea before the tsunami. Subsequently, the tsunami transported it onto the cliff top (Fig. 3b). Coral fragments and shells have been reported to be attached to the OI boulder (Kato 1989a; Nakaza et al. 2015), but these facts do not support determination of the exact process which occurred. The notch retreat point, the deepest point of the notch, is generally formed near the mean sea level to the high tide level (Pirazzoli 1986). Given that the height from the top of the OI boulder to its retreat point is about 4 m (with the upper part of the OI boulder originally being the lower part of the notch because the boulder was deposited upside down) and that the tidal range in the Sakishima Islands is about 2 m (Hongo and Kayanne 2009), the top of the OI boulder might have been located originally under 3 m water depth. Therefore, corals could have attached to the OI

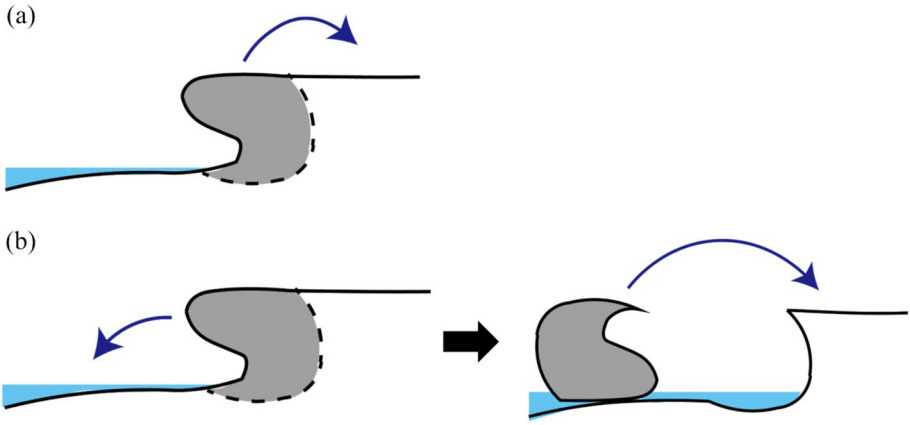

Fig. 3 **a** Schematic illustration of the case in which a part of the sea cliff was transported onto the cliff top by the tsunami. **b** Schematic illustration of the case in which the boulder had already detached from the cliff and was on the coral reef before the tsunami; later, the tsunami transported it onto the cliff top

boulder even if it was transported directly onto the cliff top from the cliff edge. Regarding the *Tridacna* fossil found on the notch part of the OI boulder (Nakaza et al. 2015), it could also have been attached there even if the boulder was transported directly from the cliff edge because *Tridacna* can live in the intertidal zone (Poutiers 1998). The notch part was located originally near the mean sea level (Pirazzoli 1986). As discussed above, it cannot be ascertained which scenario is the more reasonable. Therefore, we examined both scenarios for this study.

3 Methods

3.1 3D measuring the OI boulder

To estimate the precise size of the tsunami using tsunami boulders and numerical models (e.g., Imamura et al. 2008; Nandasena et al. 2011), the shape and volume of boulders must be estimated accurately because these models require information about the boulder shape (e.g., Engel and May 2012; Nandasena et al. 2022). Traditionally, the boulder volume has been estimated by measuring the three axes with tape during field surveys and by assuming the boulder shape to be rectangular or ellipsoidal. However, this method tends to overestimate the actual volume; moreover, it cannot capture the true shape accurately (Engel and May 2012; Nandasena et al. 2022; Nakata et al. 2023). In fact, Engel and May (2012) reported that this traditional method can overestimate the actual volume by approximately 2.5 times.

To address the shortcomings of conventional methods, this study employed high-precision 3D surveying using light detection and ranging (LiDAR). Specifically, we used the LiBackPack GC50 (GreenValley International, USA) as LiDAR equipment. This equipment, which we used for our earlier research (Nakata et al. 2023; Kasai et al. 2024), is useful to visualize huge boulders. We used the GreenValley LiFuer-BP to perform post-processing and to produce point cloud data. Subsequently, a 3D model was created from

the point cloud data using software (Agisoft Metashape Professional ver. 2.1.1; Agisoft 2024).

3.2 Tsunami numerical calculation

To calculate the boulder movement onto the cliff top from the cliff bottom or cliff edge, the vertical velocity of the tsunami should be considered because vertical acceleration is extremely important for this movement (Noormets et al. 2004; Watanabe et al. 2019; Watanabe and Arikawa 2023). However, tsunami numerical calculations that include vertical flow across the entire wide area require immense computational resources. Therefore, we used nonlinear long-wave theory for tsunami propagation in the open ocean up to a depth of 90 m, and cross-sectional two-dimensional calculations using extended Navier–Stokes equations for coastal areas. Both calculations are conducted using a Cartesian coordinate system.

3.2.1 Tsunami numerical calculation for open ocean

We used the TUNAMI-N2 model (Goto et al. 1997; Imamura et al. 2006) for tsunami propagation calculations in the open ocean. Modeling details are the same as those reported by Nakata et al. (2024). The governing equations are based on nonlinear long-wave theory, as presented in Eqs. (1)–(3).

$$\frac{\partial \eta}{\partial t} + \frac{\partial M}{\partial x} + \frac{\partial N}{\partial y} = 0 \tag{1}$$

$$\frac{\partial M}{\partial t} + \frac{\partial}{\partial x}\left(\frac{M^2}{D}\right) + \frac{\partial}{\partial y}\left(\frac{MN}{D}\right) + gD\frac{\partial \eta}{\partial x} + \frac{gn^2M\sqrt{M^2+N^2}}{D^{7/3}} = 0 \tag{2}$$

$$\frac{\partial N}{\partial t} + \frac{\partial}{\partial x}\left(\frac{MN}{D}\right) + \frac{\partial}{\partial y}\left(\frac{N^2}{D}\right) + gD\frac{\partial \eta}{\partial y} + \frac{gn^2M\sqrt{M^2+N^2}}{D^{7/3}} = 0 \tag{3}$$

These governing equations are solved numerically using the staggered leap-frog method (Goto et al. 1997; Imamura et al. 2006). In the equations, η represents the water level. M and N respectively denote fluxes in the x and y directions. Also, t denotes time, g (=9.8 m/s^2) stands for gravitational acceleration, and D represents the total water depth. Additionally, n expresses Manning's coefficient, which was set as $n=0.025$ m$^{-1/3}$/s according to the Japan Society of Civil Engineers (2002). The calculation time was set as 1 h after the earthquake because the maximum wave, which is crucially important when discussing the boulder movement, reached the Sakishima Islands within at least 1 h (Nakata et al. 2024). The time step was set as 0.05 s to ensure stable calculations. Seafloor deformation by the fault model was calculated using the method reported by Okada (1985). Here we computed both vertical and horizontal deformation (Tanioka and Satake 1996). A nested grid system was used for the tsunami calculations. The spatial grid size of the bathymetry data was reduced from offshore to the coast. The grid sizes were set to 810 m (Region 1), 270 m (Region 2), 90 m (Region 3), 30 m (Region 4), and 10 m (Region 5) (Fig. 4). According to historical documents, the Meiwa tsunami occurred around 8 a.m. on 24 April 1771, at which time the tide level was approximately equal to the mean sea level (Goto et al. 2010). Therefore, the calculations used for this study were performed assuming the tidal level to be at mean sea level.

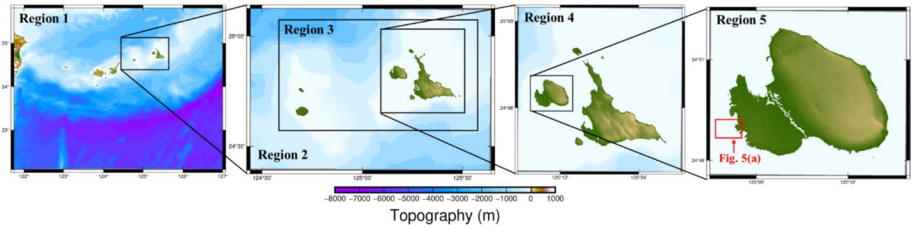

Fig. 4 Nested grids used in this study. Spatial grid sizes of the domains are 810 m (Region 1), 270 m (Region 2), 90 m (Region 3), 30 m (Region 4), and 10 m (Region 5). After Nakata et al. (2024). The red box shows the drawn area of Fig. 5a

3.2.2 Tsunami numerical calculation for coastal area

In coastal areas, we used software (CADMAS-SURF; Coastal Development Institute of Technology 2008) for cross-sectional two-dimension calculation. CADMAS-SURF is a numerical wave-tank flume program based on the extended Navier–Stokes equations for two-dimensional incompressible viscous fluid, with continuity equations and a porous model (Sakakiyama et al. 1990) as the fundamental equations. The model can reasonably simulate wave transmission and wave breaking processes over coral reef topography (Watanabe et al. 2023). The governing equations are presented below (Coastal Development Institute of Technology 2008).

$$\frac{\partial \gamma_x u}{\partial x} + \frac{\partial \gamma_z w}{\partial z} = S_\rho \tag{4}$$

$$\begin{aligned} &\lambda_v \frac{\partial u}{\partial t} + \frac{\partial \lambda_x uu}{\partial x} + \frac{\partial \lambda_z wu}{\partial z} \\ &= -\frac{\gamma_v}{\rho}\frac{\partial p}{\partial x} + \frac{\partial}{\partial x}\left\{\gamma_x \nu_e\left(2\frac{\partial u}{\partial x}\right)\right\} + \frac{\partial}{\partial z}\left\{\gamma_z \nu_e\left(\frac{\partial u}{\partial z} + \frac{\partial w}{\partial x}\right)\right\} - D_x u + S_u - R_x \end{aligned} \tag{5}$$

$$\begin{aligned} &\lambda_v \frac{\partial w}{\partial t} + \frac{\partial \lambda_x uw}{\partial x} + \frac{\partial \lambda_z ww}{\partial z} \\ &= -\frac{\gamma_v}{\rho}\frac{\partial p}{\partial z} + \frac{\partial}{\partial x}\left\{\gamma_x \nu_e\left(\frac{\partial w}{\partial x} + \frac{\partial u}{\partial z}\right)\right\} + \frac{\partial}{\partial z}\left\{\gamma_z \nu_e\left(2\frac{\partial w}{\partial z}\right)\right\} - D_z w + S_w - R_z - \gamma_v g \end{aligned} \tag{6}$$

In these equations, t represents time; also, x and z respectively denote the horizontal and vertical coordinates. Additionally, u and w are the horizontal and vertical flow velocities. Regarding other variables, ρ (=1.025 g/cm^3) denotes the density of water, p expresses pressure, ν_e represents the sum of molecular kinematic viscosity and eddy viscosity, g (=9.8 m/s^2) denotes gravitational acceleration, and γ expresses the porosity. Also, γ_x and γ_z respectively stand for the horizontal and vertical area transmittance. λ_v, λ_x, and λ_z are represented using the inertia force coefficient C_M as shown below.

$$\lambda_v = \gamma_v + (1 - \gamma_v) C_M \tag{7}$$

$$\lambda_x = \gamma_x + (1 - \gamma_x) C_M \tag{8}$$

$$\lambda_z = \gamma_z + (1 - \gamma_z) C_M \tag{9}$$

Therein, D_x and D_z are coefficients for the energy damping area. Also, S_p, S_u, and S_w represent source terms for the wave-making source. In addition, R_x and R_z denote drag forces from the porous model. They can be calculated as presented below.

$$R_x = \frac{1}{2} \frac{C_D}{\Delta x} (1 - \gamma_x) u \sqrt{u^2 + w^2} \tag{10}$$

$$R_z = \frac{1}{2} \frac{C_D}{\Delta z} (1 - \gamma_z) w \sqrt{u^2 + w^2} \tag{11}$$

In those equations, C_D is the drag coefficient. Also, Δx and Δz denote the horizontal and vertical grid sizes. For this study, Δx and Δz were set respectively to 3 m and 1 m. The time step was set automatically according to the CFL condition. All boundary conditions were set as free boundaries. The free surface of the water was calculated using the volume of fluid (VOF) method (Hirt and Nichols 1981).

We used cross-sectional bathymetry data extracted from 10 m mesh data (Region 5 in Fig. 4) along the cross-sectional line shown in Fig. 5 for CADMAS-SURF calculation. The cross-sectional line was set to align with the tsunami wave direction (Supplementary Fig. S1). In addition, we added a wave damping area (740 m) to the land side end of the bathymetry data (Fig. 5). This damping area is a virtual topography to mitigate the influence of reflection waves from the boundary at the computational area. For this calculation, the tsunami behavior on the seaward side of the cliff face is particularly important. The area behind the cliff face is flat for over 400 m. Therefore, wave reflection was unlikely to occur. Furthermore, an airport has been constructed more than 420 m inland from the cliff, making it impossible to ascertain the original topography of the area (Supplementary Fig. S2). Therefore, calculating the tsunami behavior in inland areas is unnecessary. For this reason, to reduce computational costs, a damping area was set up for the calculations used for this study. The input wave conditions were derived

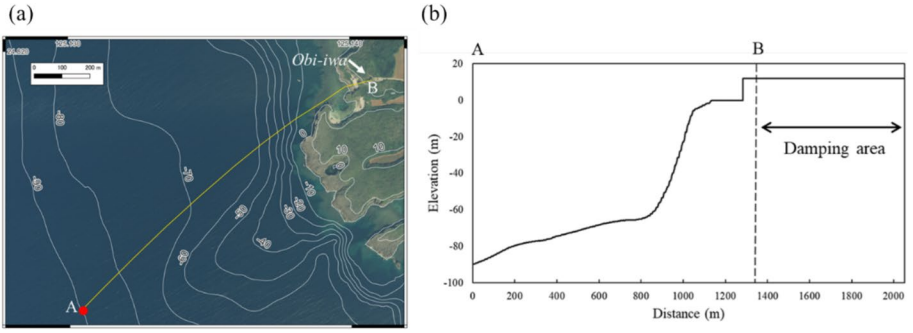

Fig. 5 **a** Aerial photograph of the area around the OI boulder taken in 2019. This photograph was provided by the Geospatial Information Authority of Japan. This area is shown in Fig. 4. The contour level in this figure is 10 m. The contour is made from 10 m mesh bathymetry and topography data (Region 5 in Fig. 4). The yellow line shows the cross-section to extract bathymetry for CADMAS-SURF. The red point shows the point at which we extracted the water level and velocity calculated using TUNAMI-N2 for the input wave conditions of CADMAS-SURF. **b** Cross-sectional bathymetry data used in CADMAS-SURF. At the land side end of the bathymetry data extracted from the cross-section shown in Fig. 5a, we added the damping area

from the water level and velocity calculated using TUNAMI-N2 at a depth of 90 m offshore of OI boulder (Fig. 5).

3.3 Boulder transport calculation

As described earlier, the initial position of the OI boulder is not well constrained. There are two possible initial positions: at the base of the cliff and at the cliff edge. Therefore, for this study, we used two boulder transport models to test both scenarios.

3.3.1 Model of boulder transport from the cliff edge onto the cliff top

Consideration of the vertical forces acting on the bottom of the notch when boulders are transported from the cliff edge onto the cliff top (Watanabe et al. 2019; Watanabe and Arikawa 2023) is important. We adopted the method reported by Watanabe and Arikawa (2023) to estimate the minimum vertical velocity acting on the bottom of the notch to transport the OI boulder. Using water tank experiments and numerical simulations, they investigated the wave forces acting on the bottom of the notch when waves reached the cliff (Watanabe and Arikawa 2023). The wave forces acting on the notch bottom are divisible into two types: impulsive force and sustained force. Impulsive force is the maximum wave force exerted when the tsunami bore impacts an object (Arikawa et al. 2005). Sustained force is generated by rising water levels because of the continuous arrival of waves (Arikawa et al. 2005). Watanabe and Arikawa (2023) showed that the impulsive force is about 4–5 times the sustained force. The sustained force is roughly equivalent to buoyancy. The OI boulder density is estimated as 1.95 because the density of the Ryukyu limestone of the OI boulder is 2.40, as detailed in Chapter 4 herein, and because the porosity average of the Ryukyu limestone is 18.8% (Miyagi and Komiya 2003). Because the OI boulder density is greater than that of water, the OI boulder cannot be transported onto the cliff top by sustained force. This fact indicates that only impulsive force is involved in the transport of the OI boulder onto the cliff top (Watanabe and Arikawa 2023). According to Watanabe and Arikawa (2023), the impulsive wave pressure P acting on the notch bottom is given by the following equation.

$$P = \rho g(h - Z) + \frac{1}{2}\rho C_p u^2 \tag{12}$$

Therein, ρ denotes the water density. C_p is the pressure coefficient. Also, g represents gravitational acceleration. h stands for the water depth. Z expresses the notch height. u represents the vertical flow velocity. The value of C_p (= 1.38) is adapted from Watanabe and Arikawa (2023).

The wave force acting on the bottom of the notch can be calculated by multiplying P by the projected area of the notch bottom A, assuming that the same pressure is used for the entire area of the notch bottom. If this force is greater than the boulder weight, then the wave can transport the boulder. From Eq. (12), the condition required to lift the boulder can be described as shown below (Watanabe et al. 2022).

$$P \times A \geq V\rho_s g \tag{13}$$

In that equation, V denotes the boulder volume; ρ_s expresses the boulder density. Because the impulsive force acts at the moment when the wave hits the notch, it is

reasonable to assume $h = Z$. Then, the minimum vertical flow velocity u' required to lift the boulder is given as the following equation.

$$u' = \sqrt{\frac{2V\rho_s g}{\rho C_p A}} \tag{14}$$

For this study, the volume of the OI boulder and the projected area of the notch bottom of the OI boulder were obtained from the 3D model. Because the OI boulder is upside down (Nakaza et al. 2015; Rixhon 2020), the lower part of the notch of the OI boulder was originally the upper part of the notch and was impacted by waves. Furthermore, the retreat point of the notch on the OI boulder from the ground is about 6 m. In fact, the height of the retreat point (Fig. 2f) corresponds to the mean sea level to the high tide level (Pirazzoli 1986). Therefore, the bottom area of the notch of the OI boulder affected by the vertical flow was originally at an elevation of approximately 0–6 m. Consequently, the maximum vertical flow velocity on the cliff face at an elevation of 0–6 m was output from CADMAS-SURF. Because the impulsive force duration was extremely short (Arikawa et al. 2005; Watanabe and Arikawa 2023), the data were output at every time step to ascertain the impulsive wave pressure.

If the maximum vertical flow velocity at the cliff face at 0–6 m elevation exceeded the minimum vertical flow velocity required to lift the OI boulder obtained from the Eq. (14), then we judge that the OI boulder could have been transported onto the cliff top. We assumed the OI boulder density (ρ_s) to be 1.95 as described above.

3.3.2 Model of boulder transport from the cliff bottom onto the cliff top

We used the boulder transport model proposed by Watanabe et al. (2019) to calculate its transport onto the cliff top from the cliff bottom. This boulder transport model, a forward model, includes not only horizontal forces but also vertical forces. The accuracy was validated based on comparison of laboratory experiments and numerical simulation results (Watanabe et al. 2019). With this model, the horizontal and vertical movements of boulders are calculated using the following equations in Cartesian coordinates.

$$\rho_s V\ddot{x} = F_{mx} - F_b - F_g \tag{15}$$

$$\rho_s V\ddot{z} = F_{mz} - F_l - F\prime_g \tag{16}$$

Therein, x and z respectively denote the horizontal and vertical coordinates of the boulder. Also, ρ_s signifies the boulder density; V stands for the volume of the boulder. F_{mx} , F_b, and F_g respectively represent the fluid force in the horizontal direction (= drag force + inertial force), friction force, and gravity. F_{mz} , F_l, and F'_g respectively denote the fluid force in the vertical direction, lift force caused by horizontal flow, and gravity. These forces are expressed by the following equations.

$$F_{mx} = C_{Dx}\frac{1}{2}\rho_f(u-\dot{x})|u-\dot{x}|A_h + \rho_f C_{Mx}\frac{Du}{Dt}V - \left(C_{Mx}-1\right)\rho_f\ddot{x}V \tag{17}$$

$$F_b = \mu\left(\rho_s - \rho_f\right)Vgcos\theta\frac{\dot{x}}{|\dot{x}|} \tag{18}$$

$$F_g = \left(\rho_s - \rho_f\right) Vgsin\theta \tag{19}$$

$$F_{mz} = C_{Dz}\frac{1}{2}\rho_f(w-\dot{z})|w-\dot{z}|A_v + \rho_f C_{Mz}\frac{Dw}{Dt}V - \left(C_{Mz}-1\right)\rho_f \ddot{z}V \tag{20}$$

$$F_l = \frac{1}{2}\rho_f C_l(u-\dot{x})^2 A_l \tag{21}$$

$$F\prime_g = \left(\rho_s - \rho_f\right) Vg \tag{22}$$

In those equations, u and w respectively represent the flow velocities in the horizontal and vertical directions at the position of the boulder. ρ_f (=1.025 g/cm^3) denotes the water density, and g (=9.8 m/s^2) represents gravitational acceleration. Also, A_h and A_v respectively denote the projected areas of the boulder in the horizontal and vertical directions to the water flow. Additionally, A_l stands for the projected area of the boulder for lift force. θ stands for the ground slope at the position of the boulder. C_l is the lift coefficient. C_{Dx} (=1.05) and C_{Mx} (=1.67) respectively represent the drag coefficient and inertial force coefficient in the x direction. Also, C_{Dz} (=1.6) and C_{Mz} (=2.5) respectively represent the drag coefficient and inertial force coefficient in the vertical direction. C_l is expressed by the equation presented below (Watanabe et al. 2019). Watanabe et al. (2019) inferred the empirical relation of Eq. 23 using experimentally obtained data reported by Malavasi and Guadagnini (2007).

$$C_l = -0.57\ln\left(\frac{h_b}{s}\right) + 0.48 \tag{23}$$

In that equation, h_b denotes the boulder position in the vertical direction; s stands for the boulder height.

In the equation below, μ is the friction coefficient. When the boulder is stationary, the static friction coefficient μ_s (=0.75) is applied. While the boulder is moving, the friction coefficient is calculated using the following equations.

$$\mu = \frac{2.2}{\beta^2+2.2}\mu_0 \tag{24}$$

$$\beta^2 = \frac{\dot{x}^2}{(1-\rho_f/\rho_s)gd} \tag{25}$$

The equations above represent an empirically derived friction coefficient that is dependent on velocity, as proposed by Imamura et al. (2008). As the flow velocity increases, the transportation mode changes. The contact time with the ground and friction decreases (Imamura et al. 2008). Here, d denotes the short axis of the boulder. Also, μ_0 (=0.71) is the dynamic friction coefficient. If the boulder is lifted off the ground, then it is assumed that F_b=0 and F_g=0. The phenomenon of boulder lifting cannot be represented by the variable friction coefficient in Imamura et al. (2008), which uses the assumption that the boulder moves only on the ground. Therefore, when the boulder is lifted because of vertical forces, the friction force (F_b) should be set as zero separately from the variable friction coefficient. The values for μ_s and μ_0 were determined as described by Imamura et al. (2001). The values of C_{Dx} , C_{Mx} , C_{Dz} , and C_{Mz} were adapted from Watanabe et al. (2019). The initial position of the boulder was set at distances of 0 m, 20 m, 40 m, 60 m, 80 m, and 100 m from the cliff edge because the exact position is unknown. The boulder

shape information (V, d, A_h, A_v, A_l) used for the calculation was obtained from the 3D model. Because the long axis is usually perpendicular to the direction of the current during transportation (Imamura et al. 2008), the projected area to the horizontal flow (A_h) was taken as the projected area of the 3D model to the plane formed by the long and height axes. A_v and A_l were also taken as the projected areas to the plane formed by the long and short axes. Furthermore, results from CADMAS-SURF were output at 0.1 s intervals every 6 m in both the horizontal and vertical directions. These outputs were used as inputs for this boulder transport model. We assumed the density of the OI boulder (ρ_s) as 1.95, as in the other model.

3.4 The 1771 Meiwa tsunami wave source model

We used the 1771 Meiwa tsunami source model proposed by Nakata et al. (2024). This model incorporates the assumption of an earthquake along the Ryukyu Trench as the tsunami source. The location of this tsunami wave source model is shown in Fig. 1(b). Table 1 presents the fault parameters.

4 Results

4.1 3D measuring of the OI boulder

The 3D model of the OI boulder made from the LiDAR survey is shown as Fig. 6. The OI boulder volume calculated from the 3D model was 1730 m^3. The three axes' lengths of the 3D model were 19.8 × 18.0 × 12.3 m if one assumes a rectangular box folding this boulder. The density was measured at 2.40 g/cm^3 using Archimedes' principle. Assuming this density, the OI boulder weighs 4152 tons. The average porosity of the Ryukyu limestone was reported as 18.8% (Miyagi and Komiya 2003). If one adopts this porosity, then the OI boulder weight can be estimated as 3374 tons.

The projected area of the 3D model to the plane formed by the long and height axes is 185 m^2; that of the 3D model to the plane formed by the long and short axes is 263 m^2 (Fig. 6b, c). These values will be applied for boulder transport modeling.

4.2 Tsunami numerical calculation

The tsunami propagation calculation results obtained using the TUNAMI-N2 model are presented in Fig. 7. The tsunami generated along the Ryukyu Trench propagated northwestward. The first receding wave reached the southern coast of Miyako Island around 850 s (Fig. 7a). Between Tarama Island and Miyako Island, there is a narrow submarine channel where channel the wave refracts and begins to head toward Shimoji Island and

Table 1 Fault parameters of the Meiwa tsunami source model proposed by Nakata et al. (2024)

Latitude (°)	Longitude (°)	Length (km)	Width (km)	Strike (°)	Dip (°)	Rake (°)	Slip (m)	Depth (km)	Mw
23.667	126.162	225	30	255	12	90	30	5	8.49

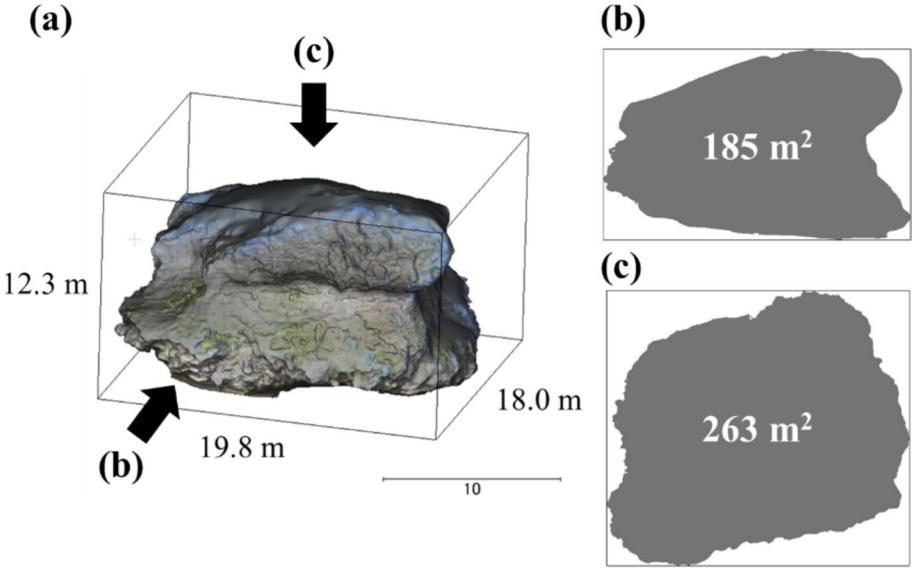

Fig. 6 **a** The 3D model of the OI boulder. **b** Projected area to the long axis × height axis plane. **c** Projected area to the long axis × short axis plane

Tarama Island (Fig. 7b). Subsequently, at approximately 1650 s, immediately before the wave reached Shimoji Island, the wave height increased remarkably offshore near the OI boulder compared to neighboring areas (Fig, 7b).

Results of the waveforms calculated using TUNAMI-N2 at the offshore point near the OI boulder, as shown in Fig. 5, are shown in Fig. 8. The first wave was the largest, with a maximum water level of approximately 14.1 m. Because the first wave is the largest and most likely to move the boulder, the waveform from 1000 to 3000 s, including the first wave, was used as input data for CADMAS-SURF calculations. The calculation results of CADMAS-SURF, when the first wave reached the cliff, are presented in Fig. 9. After the wave reached the coral reef, the shallow water caused deformation of the leading edge of the wave and formed a bore with a water level of about 21.3 m (Fig. 9). Then, the bore impacted the cliff. The water splashed vertically. Immediately after the first wave impacted the cliff, the vertical velocity on the cliff face increased rapidly at around 1738s, reaching maximum velocity of 32.9 m/s (Fig. 10). This rapidly increasing vertical velocity corresponds to impulsive force. Thereafter, the vertical velocity decreased gradually.

4.3 Boulder transport model

4.3.1 Boulder transport from the cliff edge onto the cliff top

The projected area of the notch bottom of the OI boulder as calculated from the 3D model was 87.3 m^2 (Fig. 11). Because the OI boulder notch is upside down (Nakaza et al. 2015; Rixhon 2020), the lower part of the notch was impacted by the wave. Therefore, we calculated the projected area of the lower part of the notch (Fig. 11). In addition, as described above, the OI boulder volume is 1730 m^3, with 2.40 g/cm^3

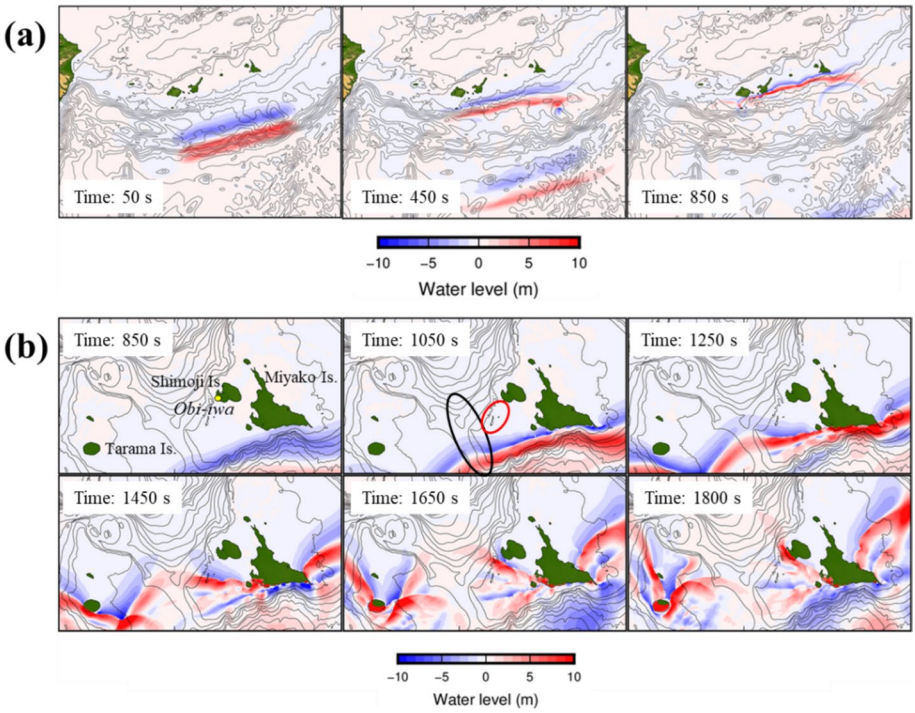

Fig. 7 **a** Results of tsunami propagation calculations using TUNAMI-N2 in Region 1 (Fig. 4). Time represents the elapsed time since the earthquake occurrence. **b** Results of tsunami propagation calculations using TUNAMI-N2 in Region 3 (Fig. 4). The black circle shows a deep area. The red circle shows a shallow area

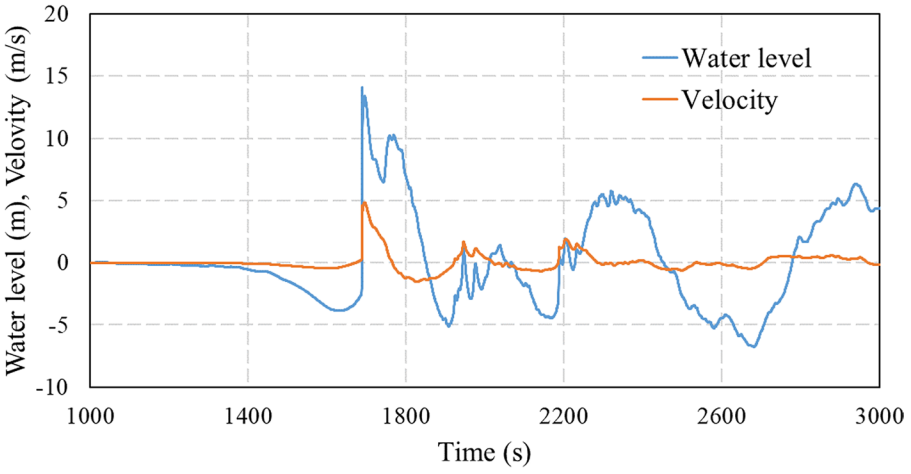

Fig. 8 Calculated waveforms of the Meiwa tsunami source model (Nakata et al. 2024) at a site offshore of OI boulder (water depth: 90 m) (Fig. 5a) by TUNAMI-N2. The horizontal axis shows the time after the earthquake happened. Positive values for the velocity show onshore flow. Negative values denote the offshore flow

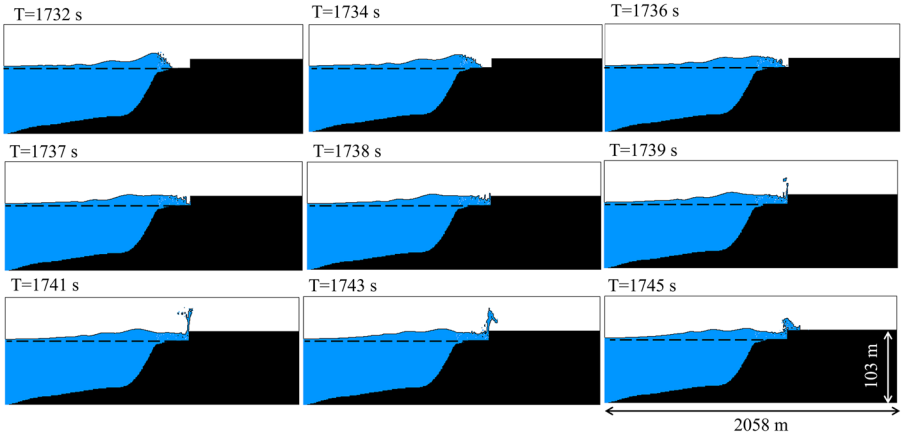

Fig. 9 Tsunami calculation results obtained using CADMAS-SURF. The dotted line represents elevation of 0 m. The vertical direction is drawn five times longer than the horizontal direction. Times in the figure represent the time after the earthquake happened

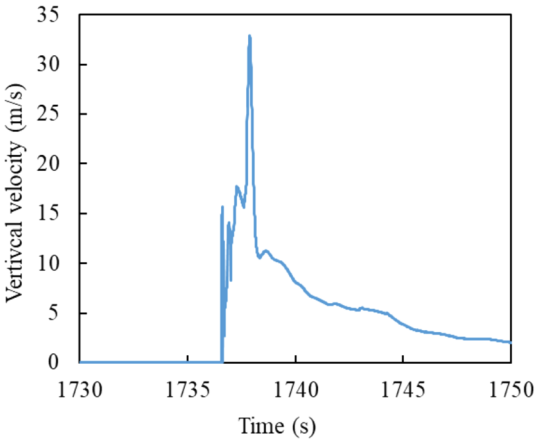

Fig. 10 Time variation of vertical velocity at the cliff face during the first wave impact. The times in the figure represent the time after the earthquake happened

density and porosity of 18.8% (Miyagi and Komiya 2003). Using these values and using Eq. (14), we estimated the minimum vertical velocity sufficient to transport the OI boulder onto the cliff top as 23.1 m/s.

4.3.2 Boulder transport from the cliff bottom onto the cliff top

Figure 12 presents results of boulder transport calculations obtained using the model reported by Watanabe et al. (2019) when the first wave reached the cliff. Not all boulders can be transported higher than the cliff height by the Meiwa tsunami (Fig. 12).

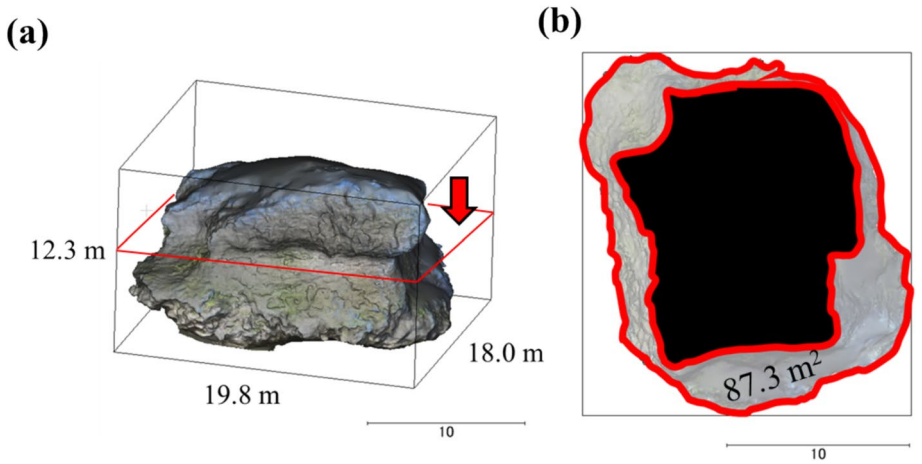

Fig. 11 Cross-sectional cut at the height of the retreat point of the OI boulder is shown in panel (**a**); a projection from the direction indicated by the red arrow is shown in panel (**b**). The black filled area represents the OI boulder interior. The area within the red line represents the bottom area of the notch where the wave impacts

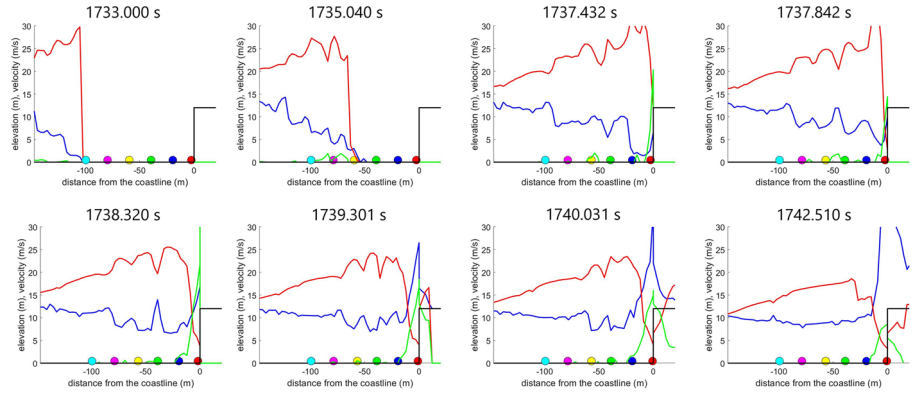

Fig. 12 Results of the boulder transport model from the cliff bottom to the cliff top when the first wave reached the cliff. The red line shows the water level. The blue line represents the horizontal flow velocity. The green line shows the vertical flow velocity. Horizontal and vertical velocities are averaged values in the height direction. Circles show the boulder positions. The times shown in the figure represent the time after the earthquake struck

5 Discussion

5.1 The 3D model of the OI boulder

The lengths of the three axes from earlier studies conducted using conventional methods were 14×14×9 m (Kato 1989b). By contrast, the lengths of the three axes from the 3D survey using the LiDAR equipment in the present study were 19.8×18.0×12.3 m. Therefore, the maximum difference in the length of the three axes between the earlier study

and this study is greater than 5 m. This difference is probably attributable to the difficulty of measuring the length of each axis of very large boulder accurately using a tape measure in the field, as well as the challenge of accurately determining the orientation of the long and short axes (Nakata et al. 2023). In addition, regarding the weight, Kato (1989b) estimated the OI boulder to be 2500 tons, but the present study estimated it to be 3374 tons even when considering the porosity. This value is 1.35 times larger than the earlier estimation. These differences emphasize the importance of 3D surveying of extremely large boulders.

The OI boulder weights estimated from this study are greater than those of any other large tsunami boulders that have ever been reported worldwide (2000 tons, French Polynesia (Bourrouilh-Le Jan and Talandier 1985; Etienne et al. 2014; Terry et al. 2021); 1600 tons, Tonga (Frolich et al. 2009); 772 tons, Kiribati (Terry et al. 2021); 700 tons, Western Australia (Playford 2014)). The OI boulder is apparently the world's largest tsunami boulder ever reported.

5.2 Age and source of the tsunami which transported the OI boulder

We examined whether the OI boulder might have been transported onto the cliff top by the Meiwa tsunami. If the initial position of the OI boulder is assumed as the cliff bottom, then the Meiwa tsunami could not have transported it onto the cliff top (Fig. 12). However, the maximum vertical velocity on the cliff face by the Meiwa tsunami is 32.9 m/s (Fig. 10), which corresponds to the impulsive force. This value is much higher than the minimum vertical flow velocity (23.1 m/s) necessary to lift the OI boulder from the cliff edge. The maximum flow velocity on the cliff face of the notch is 32.9 m/s, so the OI boulder could be transported if the notch area were larger than 40.4 m^2, according to Eq. (14). This value is approximately half of the whole notch area (87.3 m^2). Because the notch must be exposed to wave action for it to form, it is unlikely that about half of the notch area was hidden by something. Therefore, we infer that if the initial OI boulder position is the cliff edge, the Meiwa tsunami could have transported it onto the cliff top. However, it is noteworthy that we can only estimate whether the boulder starts to move, or not, using this method, and cannot discuss its subsequent movement. Calculating the subsequent movement, requires computation of the interaction between the boulder and fluid. This interaction requires the use of smoothed particle hydrodynamics (SPH) (Zainali and Weiss 2015) or a numerical system that combines a flow calculation model and a structure-foundation simulator (e.g., Hamaguchi et al. 2011), which is calculated using finite element method (FEM) or distinct element method (DEM) (Arikawa et al. 2019). However, applying these methods at a real scale requires considerable amounts of computational resources. Moreover, it is beyond the scope of this study. Therefore, this study examined only the initiation of the boulder movement. Moreover, rotational moments of the boulder around the cliff edge must be considered. This consideration requires the use of a model that incorporates angular motion equations. These three-dimensional calculations and angular motion calculations remain a subject for future work. In addition, although horizontal forces act on the boulder in real phenomena, this model considers only the vertical force. However, such forces act to make it easier to move the boulder. Therefore, ignoring these phenomena does not affect our conclusions.

Then, when was the OI boulder deposited onto the cliff? Was it during the 1771 Meiwa tsunami or during some earlier event between 700 years ago and 1771? Historical documents describing the 1771 Meiwa tsunami and its aftermath report the deposition of large boulders equivalent to the OI boulder onto the cliff top on the coast of Shimoji Island

(Kato 1989b). This study was able to show that the Meiwa tsunami could have transported the OI boulder. Therefore, it is reasonable to consider that the Meiwa tsunami transported the OI boulder.

However, as discussed in Chapter 2, as inferred from the geological records and legend, 1 to 2 large tsunamis might have struck Shimoji Island between 700 years ago and 1771. Therefore, one cannot fully rule out the possibility that the OI boulder was transported by those tsunami waves. Nevertheless, at least we can infer that it is not necessary to assume a significantly larger scale tsunami than the Meiwa tsunami.

5.3 Effects of bathymetry on tsunami size offshore of the OI boulder

Kawana and Nakata (1994) inferred that tsunami boulders on Shimoji Island were transported by a tsunami originating from the Okinawa Trough, not the Ryukyu trench side, because tsunami boulders, including the OI boulder, are concentrated on the west to north coast of Shimoji Island. However, results of this study indicate that the Meiwa tsunami which originated from the Ryukyu Trench can transport the OI boulder. This finding suggests that assuming an unknown large tsunami originating from the Okinawa Trough is not necessary to explain the tsunami boulder distribution at Shimoji Island.

Then, how did a wave large enough to transport the OI boulder, which does not face the Ryukyu trench side, reach the west coast of Shimoji Island by the earthquake along the Ryukyu trench?

The bathymetric effects for tsunami propagation are a potential cause. Nakata et al. (2024) presented results of tsunami ray tracing analysis (Satake 1988) for their Meiwa tsunami source model. The tsunami propagation direction can be represented by tsunami rays using this analytical method. The tsunami ray concentration indicates that the bathymetric characteristics concentrate the tsunami energy (Satake 1988). Tsunamis travel faster in deeper water and refract toward shallower areas. Consequently, under these certain bathymetric settings, the bathymetry causes the concentration of tsunami energy. Figure 13 shows that the tsunami ray was concentrated offshore of the OI boulder and shows that the maximum water level was also higher than that of the surrounding area. These results suggest that the tsunami was concentrated offshore of the OI boulder because of bathymetry. In fact, the tsunami propagation calculations demonstrate that the narrow channel (marked with a black circle in Fig. 7b) is deeper than its surroundings, causing the waves to refract and concentrate toward Shimoji Island. In addition, in the offshore area near Shimoji Island, the region marked with a red circle in Fig. 7b offshore of the OI boulder is shallower than the surrounding area, leading to concentration of the tsunami specifically offshore of the OI boulder (Fig. 7b, 13b). Therefore, even if the wave source is located on the Ryukyu Trench side, for this pattern of tsunami propagation, the tsunami wave can be high around the OI boulder site because of the bathymetric effect. This fact in turn indicates that one need not assume the existence of an unknown tsunami from the Okinawa Trough side to explain transportation of the OI boulder.

6 Conclusion

For this study using boulder transport models, we evaluated whether the OI boulder could have been transported by the 1771 Meiwa tsunami. First, we conducted 3D measurement of the OI boulder to produce input data for boulder transport calculations.

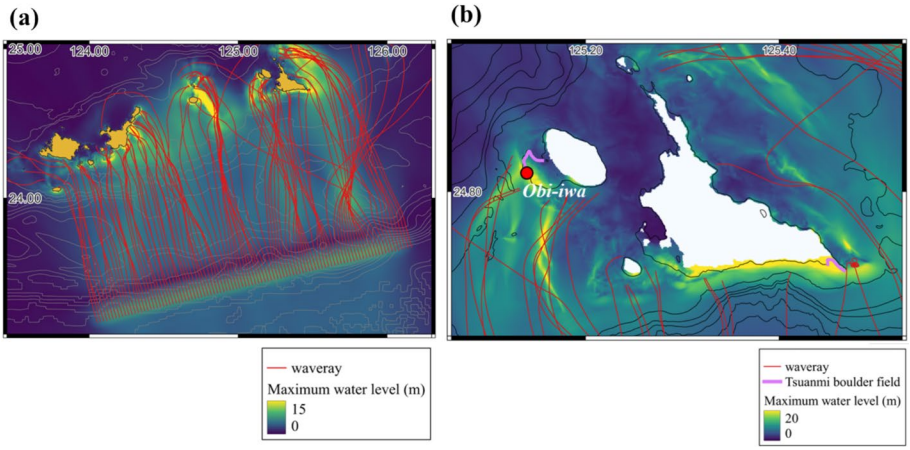

Fig. 13 Figures depict results of wave ray tracing analysis and the maximum water level distribution of the Meiwa tsunami model proposed by Nakata et al. (2024). **a** Entire Ryukyu Trench to the Sakishima Islands (results from Region 1 in Fig. 4), **b** around Shimoji Island (results from Region 4 in Fig. 4). Thick pink lines in (**b**) show the tsunami boulder distribution (Goto et al. 2010). The contour level is 500 m in (**a**) and 100 m in (**b**). These calculation results were derived from Nakata et al. (2024)

From the 3D measurements, the OI boulder was estimated as 3374 tons, indicating it as the world's largest tsunami boulder reported to date. Subsequently, we examined two scenarios for transport of the OI boulder: the cliff edge scenario and the cliff bottom scenario. If we assume that the initial position of the OI boulder was the cliff bottom, then the Meiwa tsunami would have been unable to have transported the OI boulder. However, if the initial position of the OI boulder were at the cliff edge, then the Meiwa tsunami would have been able to transport the OI boulder onto the cliff top. Indeed, the assumption that the initial position of the OI boulder was at the cliff edge sounds reasonable based on field observations.

This result indicates that a tsunami that was extremely larger than the Meiwa tsunami or some unknown tsunami from the Okinawa Trough need not be assumed. In addition, analysis of tsunami wave rays revealed that the bathymetry affected the tsunami propagation and that tsunami energy was concentrated offshore of the OI boulder. This concentration is probably the main reason why a tsunami generated at the opposite side of the island from OI boulder would still be able to transport it.

Supplementary Information The online version contains supplementary material available at https://doi.org/10.1007/s11069-025-07276-2.

Acknowledgements We appreciate Okinawa prefecture for providing topography and bathymetry data used for tsunami calculations. We used the plate boundary model proposed by Iwasaki et al. (2015), which was constructed from topography and bathymetry data by the Geospatial Information Authority of Japan (250 m digital map), Japan Oceanographic Data Center (500 m mesh bathymetry data, J-EGG500, http://www.jodc.go.jp/jodcweb/JDOSS/infoJEGG_j.html), and the Generic Mapping Tools (GMT, ver. 6.1.1) (Wessel et al. 2019) for data handling and plotting of Figures 1, 4 and 7.

Authors' contributions KG proposed the topic and designed the research. KN and MW conducted numerical calculations. KN and KG prepared an original draft. All authors participated in discussions and approved the final manuscript.

Funding Open Access funding provided by The University of Tokyo. This study was supported by the Ministry of Education, Culture, Sports, Science and Technology (MEXT) of Japan, under its third Earthquake and Volcano Hazards Observation and Research Program (Earthquake and Volcano Hazard Reduction Research), by JSPS KAKENHI Grant Number 21H04508, by SATREPS, JST/JICA, and by JST SPRING, Grant Number JPMJSP2108.

Declarations

Competing interests The authors declare that they have no competing interest.

References

Abad M, Izquierdo T, Cáceres M, Bernárdez E, Rodriguez-Vidal J (2020) Coastal boulder deposit as evidence of an ocean-wide prehistoric tsunami originated on the Atacama Desert coast (northern Chile). Sedimentology 67(3):1505–1528. https://doi.org/10.1111/sed.12570

Agisoft (2024) Agisoft Metashape Version 2.1.1. Agisoft. https://www.agisoft.com/downloads/installer/ Accessed 23 May 2024

Ando M, Kitamura A, Tu Y, Ohashi Y, Imai T, Nakamura M, Ikuta R, Miyairi Y, Yokoyama Y, Shishikura M (2018) Source of high tsunamis along the southernmost Ryukyu Trench inferred from tsunami stratigraphy. Tectonophysics 722:265–276. https://doi.org/10.1016/j.tecto.2017.11.007

Araoka D, Yokoyama Y, Suzuki A, Goto K, Miyagi K, Miyazawa K, Matsuzaki H, Kawahata H (2013) Tsunami recurrence revealed by Porites coral boulders in the southern Ryukyu Islands, Japan. Geology 41:919–922. https://doi.org/10.1130/G34415.1

Arikawa T, Yamada H, Akiyama M (2005) Study of applicability of tsunami wave force in a three-dimensional numerical wave flume. Jpn Soc Civ Eng Coast Eng 52:46–50. https://doi.org/10.20965/jdr.2021.p1286. (**in Japanese**)

Arikawa T, Chida Y, Seki K, Takagawa T, Shimosako K (2019) Development and applicability of multiscale multiphysics integrated simulator for tsunami. J Disast Res 14(2):225–234. https://doi.org/10.20965/jdr.2019.p0225

Baptista MA, Miranda PMA, Miranda JM, Victor LM (1998) Constraints on the source of the 1755 Lisbon tsunami inferred from numerical modelling of historical data on the source of the 1755 Lisbon tsunami. J Geodyn 25(1–2):159–174. https://doi.org/10.1016/S0264-3707(97)00020-3

Bourrouilh-Le Jan FG, Talandier J (1985) Major high-energy events in a reef environment: tsunamis, hurricanes and tropical cyclones and their effects on the sedimentology and geomorphology of an atoll: Rangiroa, Tuamotu (SE Pacific). Mar Geol 37(3–4):263–272. https://doi.org/10.1016/0025-3227(85)90095-7

Coastal Development Institute of Technology (2008) Research and Development of Numerical Wave Flume: CADMAS-SURF. Coastal Development Institute of Technology, Tokyo

Egashira K, Fukuda I, Kishira Y, Nishimura T (1985) Field measurement of the wave deformation on the reef. Proc Coast Eng, JSCE 32:90–94. (**in Japanese**, original title translated). https://doi.org/10.2208/proce1970.32.90

Engel M, May SM (2012) Bonaire's boulder fields revisited: evidence for Holocene tsunami impact on the Leeward Antilles. Quatern Sci Rev 54:126–141. https://doi.org/10.1016/j.quascirev.2011.12.011

Etienne S, Couchoud I, Jeanson M, Lau A, Paris R, Terry J (2014) Les risques naturels extrêmes sur les littoraux de la Polynésie française: Archives géologiques – modélisation – réduction des risques. Rapport scientifique du programme RINALPOF, Contrat de Projet Etat-Territoire 2009–2013, Université de la Polynésie française – Ecole Pratique des Hautes Etudes

Frohlich C, Hornbach MJ, Taylor FW, Shen CC, Moala A, Morton AE, Kruger J (2009) Huge erratic boulders in Tonga deposited by a prehistoric tsunami. Geology 37(2):131–134. https://doi.org/10.1130/G25277A.1

Fujita R, Goto K, Iryu Y, Abe T (2020) Millennial paleotsunami history at Minna Island, southern Ryukyu Islands, Japan. Prog Earth Planet Sci 7:53. https://doi.org/10.1186/s40645-020-00365-9

Goto K, Kawana T, Imamura F (2010) Historical and geological evidence of boulders deposited by tsunamis, southern Ryukyu Islands, Japan. Earth-Sci Rev 102:77–99. https://doi.org/10.1016/j.earscirev.2010.06.005

Goto K, Miyazawa K, Adaniya A, Kakihana S, Kugai M, Shimabukuro A, Shimabukuro N, Masaki Y, Matsushima S, Miyagi K (2012) Reevaluation of the run-up height of the 1771 Meiwa tsunami II—the Sakishima Islands. Res Rep Tsunami Eng 29:129–146 (**in Japanese**)

Goto K, Shimabukuro A (2012) Interdisciplinary researchers on the 1771 Meiwa tsunami. Kagaku 82(2):208–214. (**in Japanese**, original title translated)

Goto C, Ogawa Y, Shuto N, Imamura F (1997) IUGG/IOC Time Project, numerical method of tsunami simulation with the Leap-Frog scheme. IOC Manuals and Guides, UNESCO, Paris

Hamaguchi K, Arikawa T, Kitagawa K (2011) Analysis of deformation and fracture of seawall joint using a fluid-structure coupled system. J Jpn Soc Civ Eng Ser B2 (Coastal Eng) 67(2):I_771–I_775. (**in Japanese** with English abstract). https://doi.org/10.2208/kaigan.67.I_771

Heaton TJ, Köhler P, Butzin M, Bard E, Reimer RW, Austin WE et al (2020) Marine20—the marine radiocarbon age calibration curve (0–55,000 cal BP). Radiocarbon 62(4):779–820. https://doi.org/10.1017/RDC.2020.68

Hirabayashi S, Yokoyama Y, Suzuki A, Miyairi Y, Aze T (2017) Short-term fluctuations in regional radiocarbon reservoir age recorded in coral skeletons from the Ryukyu Islands in the north-western Pacific. J Quat Sci 32(1):1–6. https://doi.org/10.1002/jqs.2923

Hirt CW, Nichols BD (1981) Volume of fluid (VOF) method for the dynamics of free boundaries. J Comput Phys 39(1):201–225. https://doi.org/10.1016/0021-9991(81)90145-5

Hisamatsu A, Goto K, Imamura F (2014) Local paleo-tsunami size evaluation using numerical modeling for boulder transport at Ishigaki Island, Japan. Episodes 37:265–276. https://doi.org/10.18814/epiiugs/2014/v37i4/006

Hongo C, Kayanne H (2009) Holocene coral reef development under windward and leeward locations at Ishigaki Island, Ryukyu Islands, Japan. Sediment Geol 214:62–73. https://doi.org/10.1016/j.sedgeo.2008.01.011

Imamura F, Yoshida I, Moore A (2001) Numerical study of the 1771 Meiwa tsunami at Ishigaki Island, Okinawa and the movement of the tsunami stones. Proc Coast Eng JSCE 48:346–350 (**in Japanese**)

Imamura F, Yalciner AC, Ozyurt G (2006) Tsunami Modelling Manual (TUNAMI model). http://www.tsunami.civil.tohoku.ac.jp/hokusai3/J/projects/manual-ver-3.1.pdf Accessed 15 Jan 2023

Imamura F, Goto K, Ohkubo S (2008) A numerical model for the transport of a boulder by tsunami. Journal of Geophysical Research: Oceans 113(C1). https://doi.org/10.1029/2007JC004170

Iwasaki T, Sato H, Shinohara M, Ishiyama T, Hashima A (2015) Fundamental structure model of island arcs and subducted plates in and around Japan. In: AGU 2015 Fall Meet, San Francisco, Dec 14–18, T31B-2878

Izumi N, Nishizawa A, Horiuchi D, Kido Y, Goto H, Nakata T (2016) 3D bathymetric image of Nansei-Shoto Trench and its vicinity. Rep Hydrol Ocean Res 53:133–149 (**in Japanese**)

Japan Society of Civil Engineers (The Tsunami Evaluation Subcommittee, The Nuclear Civil Engineering Committee) (2002) Tsunami assessment method for nuclear power plants in Japan. Japan Society of Civil Engineers, Tokyo (**in Japanese**)

Kasai K, Yanagisawa H, Goto K (2024) Quantification of the spatial distribution of individual mangrove tree species derived from LiDAR point clouds. Prog Earth Planet Sci 11(1):21. https://doi.org/10.1186/s40645-024-00626-x

Kato Y (1989b) Yaeyama Seismic Tsunami (1771) in the Miyako Islands recorded in the newly found archives "Otoiai-gaki." Bull Coll Sci Univ Ryukyus 47:153–158 (**in Japanese with English abstract**)

Kato Y (1989a) The origin of "Obi-oiwa" on Shimoji Island in Miyako islands, Okinawa prefecture. Soc Hist Earthq Stud 5:111–115. (**in Japanese**, original title translated)

Kawana T, Nakata K (1994) Timing of Late Holocene tsunamis originated around the southern Ryukyu Islands, Japan, deduced from coralline tsunami deposits. J Geogr Jpn 103:352–376. (**in Japanese** with English abstract). https://doi.org/10.5026/jgeography.103.4_352

Kawana T, Apirazzoli P (1990) Re-examination on the Holocene emerged shorelines in Irabu and Shimoji Islands, the South Ryukyus, Japan. Quater Res (Daiyonki-Kenkyu) 28(5):419–426

Lavigne F, Morin J, Wassmer P, Weller O, Kula T, Maea AV et al (2021) Bridging legends and science: field evidence of a large tsunami that affected the Kingdom of Tonga in the 15th Century. Front Earth Sci 9:748755. https://doi.org/10.3389/feart.2021.748755

Lindquist KG, Engle K, Stahlke D, Price E (2004) Global topography and bathymetry grid improves research efforts. Eos Trans AGU 85:186. https://doi.org/10.1029/2004EO190003

Malavasi S, Guadagnini A (2007) Interactions between a rectangular cylinder and a free-surface flow. J Fluids Struct 23(8):1137–1148. https://doi.org/10.1016/j.jfluidstructs.2007.04.002

Miyagi N, Komiya Y (2003) Effective porosity and compression strength of Ryukyu limestone in Pleistocene Epoch in the Quaternary period. Sci Bull Coll Agric Univ Ryukyus 50:131–135 (**in Japanese with English title**)

Miyazawa K, Goto K, Imamura F (2012) Re-evaluation of the 1771 Meiwa tsunami source model, southern Ryukyu Islands, Japan. In: Yamada Y, Kawamura K, Ikehara K, Ogawa Y, Urgeles R, Mosher D, Chaytor J, Strasser M (eds) Advances in natural and technological hazards research, Submarine mass movements and their consequences. Springer, Heidelberg, vol 31, pp 497–506. https://doi.org/10.1007/978-94-007-2162-3_44

Nakamura M (2009) Fault model of the 1771 Yaeyama earthquake along the Ryukyu Trench estimated from the devastating tsunami. Geophys Res Lett 36:L19307. https://doi.org/10.1029/2009GL039730

Nakata K, Yanagisawa H, Goto K (2023) A new point cloud processing method unveiled hidden coastal boulders from deep vegetation. Sci Rep 13:10918. https://doi.org/10.1038/s41598-023-37985-2

Nakata K, Goto K, Yanagisawa H (2024) New source model for the 1771 Meiwa tsunami along the southern Ryukyu Trench inferred from high-resolution tsunami calculation. Prog Earth Planet Sci 11(1):28. https://doi.org/10.1186/s40645-024-00631-0

Nakaza E, Iribe T, Tokuhisa R, Miyazato N, Inagaki K (2013) Prehistorical and historical tsunamis of Ryukyu Islands estimated through tsunami depositions. J Jpn Soc Civil Eng, Ser B3 (Ocean Eng) 69:515–520. (**in Japanese** with English abstract). https://doi.org/10.2208/jscejoe.69.I_515

Nakaza E, Tokuyama R, Inagaki K (2015) Original locations of huge boulders moved by tsunami and its generation mechanism. J Jpn Soc Civil Eng, Ser B2 (Coastal Eng), 71(2):193–198. (**in Japanese** with English abstract). https://doi.org/10.2208/kaigan.71.I_193

Namegaya Y, Satake K (2014) Reexamination of the AD 869 Jogan earthquake size from tsunami deposit distribution, simulated flow depth, and velocity. Geophys Res Lett 41(7):2297–2303. https://doi.org/10.1002/2013GL058678

Nandasena NAK, Paris R, Tanaka N (2011) Reassessment of hydrodynamic equations: Minimum flow velocity to initiate boulder transport by high energy events (storms, tsunamis). Mar Geol 281(1–4):70–84. https://doi.org/10.1016/j.margeo.2011.02.005

Nandasena NAK, Scicchitano G, Scardino G, Milella M, Piscitelli A, Mastronuzzi G (2022) Boulder displacements along rocky coasts: A new deterministic and theoretical approach to improve incipient motion formulas. Geomorphology 407:108217. https://doi.org/10.1016/j.geomorph.2022.108217

Noormets R, Crook KA, Felton EA (2004) Sedimentology of rocky shorelines: 3.: hydrodynamics of megaclast emplacement and transport on a shore platform, Oahu, Hawaii. Sedimentary Geol 172(1–2):41–65. https://doi.org/10.1016/j.sedgeo.2004.07.006

Okada Y (1985) Surface displacement due to shear and tensile faults in a halfspace. Bull Seismol Soc Am 75:1135–1154. https://doi.org/10.1785/BSSA0750041135

Okamura Y, Nishizawa A, Fujii Y, Yanagisawa H (2018) Accretionary prism collapse: a new hypothesis on the source of the 1771 giant tsunami in the Ryukyu Arc. SW Jpn Sci Rep 8:13620. https://doi.org/10.1038/s41598-018-31956-8

Okinawa Prefectural Archeological Center (2017) Survey report of Shiraho-Saonetabaru cave ruins 2—summary report edition—Okinawa Prefectural Archeological Center reports 86. (**in Japanese**, original title translated). https://doi.org/10.24484/sitereports.19848

Pirazzoli PA (1986) Marine notches. In: van de Plassche O (ed) Sea-level research: a manual for the collection and evaluation of data. Geo Books, Norwich, pp 361–400. https://doi.org/10.1007/978-94-009-4215-8_12

Playford PE (2014) Recent mega-tsunamis in the Shark Bay, Pilbara, and Kimberley areas of Western Australia. J R Soc West Aust 97:173–188

Poutiers JM (1998) Bivalves. Acephala, Lamellibranchia, Pelecypoda. In: Carpenter KE, Niem VH (eds) FAO species identification guide for fishery purposes, The living marine resources of the Western Central Pacific, vol 1. FAO, Rome, pp 123–362

Rixhon G (2020) Cosmogenic nuclide dating of coarse clasts. In: Engel M, Pilarczyk J, May SM, Brill D, Garret E (eds) Geological records of tsunamis and other extreme waves. Elsevier, Amsterdam, pp 761–775. https://doi.org/10.1016/B978-0-12-815686-5.00035-3

Sakakiyama T, Abe N, Kajima R (1990) Analysis of nonlinear wave around permeable structure by porous model. Proc Coast Eng JSCE 37:554–558. https://doi.org/10.2208/proce1989.37.554. (**in Japanese**)
Satake K (1988) Effects of bathymetry on tsunami propagation: application of ray tracing to tsunamis. Pure Appl Geophys 126:27. https://doi.org/10.1007/BF00876912
Satake K, Nanayama F, Yamaki S (2008) Fault models of unusual tsunami in the 17th century along the Kuril Trench. Earth Planets Space 60:925–935. https://doi.org/10.1186/BF03352848
Shimoji, K. (2007). "Amare-mura" and a legend tsunami. Miyakojima City Mus Bull 11:1–12. (**in Japanese**, original title translated)
Sugawara D (2021) Numerical modeling of tsunami: Advances and future challenges after the 2011 Tohoku earthquake and tsunami. Earth Sci Rev 214:103498. https://doi.org/10.1016/j.earscirev.2020.103498
Sunagawa G (1994) Natural disasters in Miyako in the late early modern period. Taira City Mus Bull 1:1–17. (**in Japanese**, original title translated)
Takenaga K (1968) The classification of notch profiles and the origin of notches. J Geogr (Chigaku Zasshi) 77(6):329–341. https://doi.org/10.5026/jgeography.77.6_329. (**in Japanese**)
Tanioka Y, Satake K (1996) Tsunami generation by horizontal displacement of ocean bottom. Geophys Res Lett 23:861–864. https://doi.org/10.1029/96GL00736
Terry JP, Karoro R, Gienko GA, Wieczorek M, Lau AA (2021) Giant palaeotsunami in Kiribati: converging evidence from geology and oral history. Island Arc 30(1):e12417. https://doi.org/10.1111/iar.12417
Trenhaile AS (2015) Coastal notches: their morphology, formation, and function. Earth Sci Rev 150:285–304. https://doi.org/10.1016/j.earscirev.2015.08.003
Watanabe M, Arikawa T (2023) Elucidation of wave pressure acting on a wave-cut notch beneath a coastal cliff based on laboratory experiments and numerical modeling. Ocean Eng 270:113656. https://doi.org/10.1016/j.oceaneng.2023.113656
Watanabe M, Goto K, Imamura F, Hongo C (2016) Numerical identification of tsunami boulders and estimation of local tsunami size at Ibaruma reef of Ishigaki Island, Japan. Isl Arc 25:316–332. https://doi.org/10.1111/iar.12115
Watanabe M, Goto K, Imamura F, Kennedy A, Sugawara D, Nakamura N, Tonosaki T (2019) Modeling boulder transport by coastal waves on cliff topography: case study at Hachijo Island, Japan. Earth Surf Process Landf 44(15):2939–2956. https://doi.org/10.1002/esp.4684
Watanabe M, Kan H, Toguchi K, Nakashima Y, Roeber V, Arikawa T (2023) Effect of the structural complexity of a coral reef on wave propagation: a case study from Komaka Island, Japan. Ocean Eng 287(1):115632. https://doi.org/10.1016/j.oceaneng.2023.115632
Watanabe M, Arikawa T, Goto K (2022) Tsunami boulders teach us about mega-tsunami. Kenchiku Bousai, JBDPA 532:20–24. (**in Japanese**, original title translated)
Wessel P, Luis JF, Uieda L, Scharroo R, Wobbe F, Smith WHF, Tian D (2019) The generic mapping tools ver. 6. Geochem Geophys 20:5556–5564. https://doi.org/10.1029/2019GC008515
Yamamoto M, Taira K, Yamada K (2014) Survey Report of the Kidomari Village Ruins on Irabu and Shimoji Islands. 2011 Toyota Foundation Research Grant Program: Comprehensive Research Report on the Historical Evolution of Administrative Disaster Prevention Measures, Systems, and Policies in Okinawa and Amami Island Societies 6:21–37. (**in Japanese**, original title translated)
Zainali A, Weiss R (2015) Boulder dislodgement and transport by solitary waves: insights from three-dimensional numerical simulations. Geophys Res Lett 42:4490–4497. https://doi.org/10.1002/2015GL063712